X-ray Imaging with GEM-based detectors using Single-Pixel Imaging techniques

Matilde Simões[1,2] | A.F.V. Cortez[2] | H. Natal da Luz[2] | Pedro G. Vaz[1]

LIBPhys, Department of Physics, Rua Larga, University of Coimbra, 3004-516 Coimbra, Portugal
Institute of Experimental and Applied Physics, Czech Technical University in Prague,
Husova 240/5, 110 00 Prague 1, Czech Republic

Introduction

X-rays have proven to be an invaluable tool for noninvasive analysis in many fields ranging from basic science to medicine, engineering and security. In the last century, many advancements have been made in the field of X-ray imaging. However, there are still some limitations to be considered. X-ray radiation poses a risk to human health by harming human body tissues, so it is crucial to achieve low-dose imaging, avoiding overexposure. The X-ray detectors still present a low sensitivity and adding to that the necessity to reduce radiation exposure, the need to increase this sensitivity is imperative. All these factors, compromise the task of achieving large area high resolution X-ray imaging.

The alternative proposed in this work to possibly overcome some of these limitations is Single-Pixel Imaging (SPI). The main objective of this work is to further study the feasibility of SPI with X-ray radiation. For that, a SPI prototype was simulated in GEANT4 and built experimentally. The detector developed was a triple cascade of GEMs (Gas Electron Multiplier), quantifying its performance in gain, energy resolution and uniformity in area and in time. The set of patterns applied were based on the Hadamard matrix and 3D printed in 5mm PLA (Polylactic Acid filament) masks, testing a new material and manufacturing process for the light modulator. Measurements were performed for different acquisition times per mask, in order to obtain 4x4 pixel images.

Scientific Background

Single-Pixel Imaging

This technique relies on numerical processing power to achieve higher resolution images, instead of complex hardware. An SPI system is formed mainly by three distinct elements:

- Single-pixel detector;
- Light source;
- Light modulator/masks.

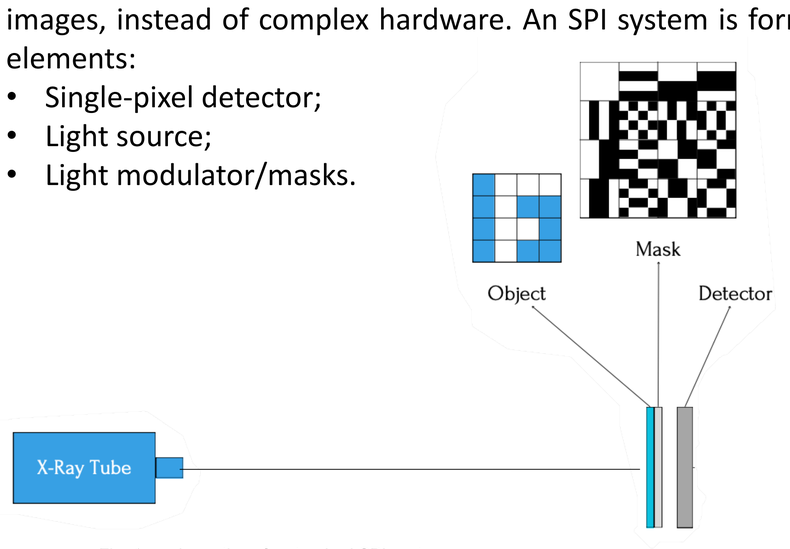

Fig. 1 – schematics of a standard SPI system.

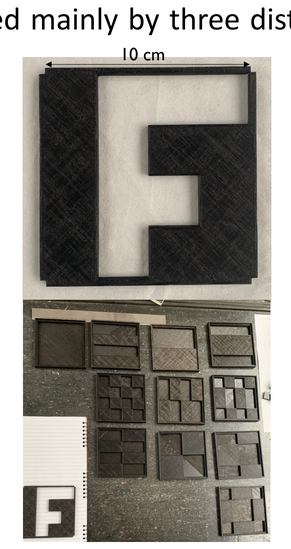

Fig. 2 – Above: printed object. Below: printed masks.

The spatial light modulator is employed to project different pre-selected patterns onto a scene, strategically chosen from a sensing matrix, enabling effective image reconstruction.

Important Concepts

- **Sensing Matrix:** based on the Hadamard matrix of order 16 (calculated with equation 1). By reshaping each line as in Figure 3, the 16 masks are obtained.
- **Reconstruction algorithm:** inverse transform, as in equation 2.

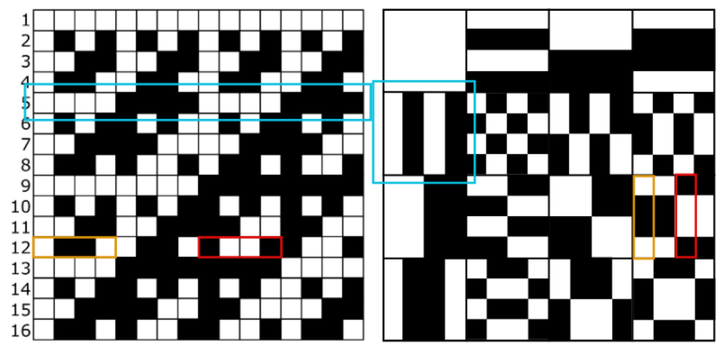

Fig. 3 – Hadamard matrix of order 16 in natural ordering with the corresponding reshaped patterns.

$$H_{2^k} = \begin{bmatrix} H_{2^{k-1}} & H_{2^{k-1}} \\ H_{2^{k-1}} & -H_{2^{k-1}} \end{bmatrix} = H_2 \otimes H_{2^{k-1}}$$

Eq. 1 – Hadamard matrix equation

$$\begin{bmatrix} x_1 \\ \vdots \\ x_n \end{bmatrix} = H^{-1} \begin{bmatrix} y_1 \\ \vdots \\ y_n \end{bmatrix} = \frac{1}{n} H \begin{bmatrix} y_1 \\ \vdots \\ y_n \end{bmatrix}$$

Eq. 2 – inverse transform reconstruction formula.

Advantages

- Cost effective alternative to multi-pixelated solutions;
- Improved geometry detector efficiency;
- Faster timing response when compared with frame-based readout;
- Reduced data storage and data transfer time;

X-ray Imaging SPI - Experimental Setup and Results

Experimental Setup

A single-pixel camera was developed to test the concept of X-ray SPI, as represented in Figure 3. The designed camera was composed of three main components/parts:

- An X-ray tube;
- A set of masks that contain the different patterns;
- A triple GEM detector, with the electronics associated comprising of a Charge-sensitive amplifier, a Shaping Amplifier and an ADC.

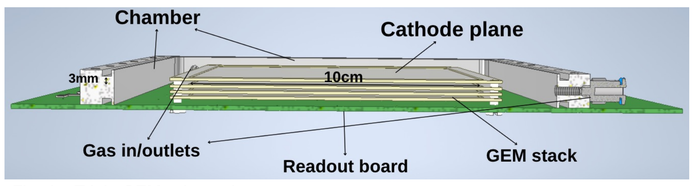

Fig. 4 – Triple GEM schematics.

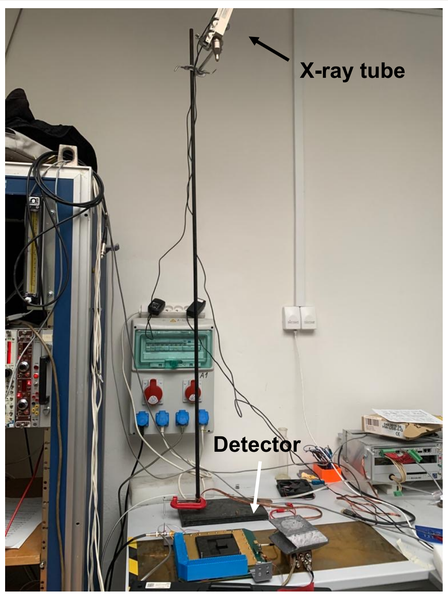

Fig. 5 – Experimental Setup.

Tab. 1 – Specifications of the triple GEM detector.

Active area	Hole size	Hole spacing	Drift gap	Transfer gaps	Induction gap	Gas
10x10cm^2	70µm	140µm	3mm	2mm	1.5mm	Ar/CO_2 (70/30)

The results are represented in Figure 6. PLA filament showed the best performance of the filaments, plus it was already available in the laboratory.

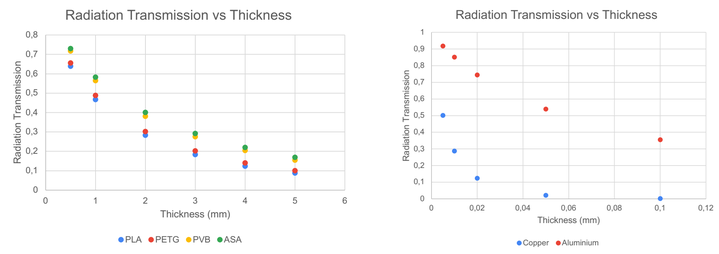

Fig. 6 – Radiation transmission as a function of thickness. Left: Polymers. Right: Metals

Reconstructed Images

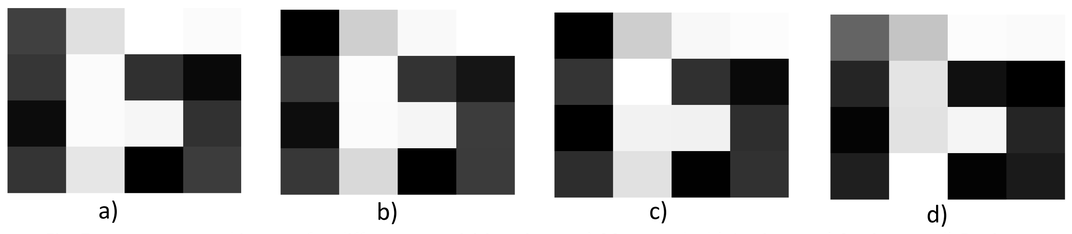

Fig. 7 – reconstructed images for different acquisition times. a) 30 seconds. b) 1 minute. c) 2 minutes. d) 5 minutes.

Mask Studies

To define the material and thickness of the masks, simulations were performed with a simplified version of the setup (Figure 5), where the mask has variable thickness and material, in order to find the optimal operating point considering:

- Transmission percentage (law of attenuation);
- Cost;
- Amount of material.

Fig. 6 – Designed Setup for the simulations.

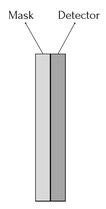

Materials
Polylactic Acid filament
Polyethylene Terephthalate Glycol filament
Polyvinyl Butyral filament
Acrylonitrile Styrene Acrylate filament
Copper
Aluminium

Thickness (mm)	
Filaments	Metals
0.5	0.005
1	0.01
2	0.02
3	0.05
4	0.1
5	

In order to evaluate in a more quantitative way, we also calculated the CNR with the following equation:

$$CNR = \frac{signal}{\sqrt{\sigma_s^2 + \sigma_b^2}} = \frac{\overline{w} - \overline{d}}{\sqrt{\sigma_w^2 + \sigma_d^2}}$$

Eq. 3 – Contrast-to-noise Ratio (CNR)

where σ_s^2 and σ_b^2 are the variances of the signal and the background, respectively and *w* and *b*, stand for white and dark pixel.

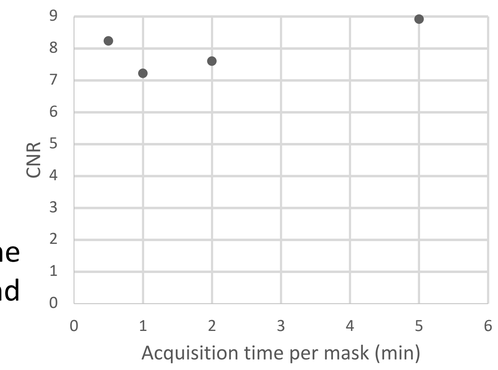

Fig. 8 – CNR as a function of acquisition time per mask.

Conclusions and Future work

The proof of concept was successfully made, both computationally and experimentally. In addition, a functional triple GEM detector was built and characterized in terms of energy resolution, detector gain and uniformity. The acquisition time per mask and the CNR did not present a clear proportional relation, due to the statistical fluctuations created by the detector. PLA filament proved to absorb enough radiation, presenting itself as an alternative to the metals usually used, reducing the total cost of the setup.
The next steps will be:

- Optimization of the printing of the masks;
- Increase of the number of pixels on the masks and the object;
- Automation of the mask-changing procedure;
- Employment of more complex reconstruction algorithms;
- X-ray fluorescence imaging applying SPI;
- X-ray SPI through a diffuse media.

References

[1] Yu-Hang He et al., High-resolution sub-sampling incoherent x-ray imaging with a single-pixel detector, *APL Photonics* 5.056102 (2020).
[2] Pedro G. Vaz et al., Re-Ordering of Hadamard Matrix Using Fourier Transform and Gray-Level Co-Occurrence Matrix for Compressive Single-Pixel Imaging in Low Resolution Images, *IEEE Access* 10 (2022).
[3] Pedro G. Vaz et al., Single-pixel imaging: concepts and application to imaging through scattering media, *ICTON* (2023).

Contact: mati.sims14@gmail.com

The authors acknowledge the support from grant GAČR GA21-21801S, Czech Republic.